Electrosorption of phenolic compounds from olive mill wastewater: Mass transport consideration under a transient regime through an alginate-activated carbon fixed-bed electrode

Amina Lissaneddine, Marie-Noëlle Pons, Faissal Aziz, Naaila Ouazzani, Laila Mandi, Emmanuel Mousset

Electrosorption of phenolic compounds from olive mill wastewater: Mass transport consideration under a transient regime through an alginate-activated carbon fixed-bed electrode

Amina Lissaneddine[1,2,3], Marie-Noëlle Pons[1], Faissal Aziz[2,3], Naaila Ouazzani[2,3], Laila Mandi[2,3], Emmanuel Mousset[1,*]

[1] *Université de Lorraine, CNRS, LRGP, F-54000 Nancy, France*

[2] *National Center for Research and Studies on Water and Energy (CNEREE), Cadi Ayyad University, B. 511, 40000, Marrakech, Morocco*

[3] *Laboratory of Water, Biodiversity, and Climate Change, Faculty of Sciences Semlalia, Cadi Ayyad University, B.P. 2390, 40000, Marrakech, Morocco*

ACCEPTED IN

JOURNAL OF HAZARDOUS MATERIALS

2022

*Contact of the corresponding author: emmanuel.mousset@cnrs.fr

Abstract

Olive mill wastewater (OMWW) is an environmentally critical effluent, specifically due to its high content of phenolic compounds (PCs), which are hazardous due to their antimicrobial activities in water. However, their properties have good health effects at suitable doses. For the first time, the electrosorption of PCs from actual OMWW has been proposed for their possible recovery as value-added compounds, while decontaminating OMWW. A bio-sourced alginate-activated carbon (AC) fixed-bed electrode was prepared based on the reuse of olive pomace solid waste as powdered AC. At the optimal AC content (1% w/v), the internal ohmic drop voltage was lower (2.26 V) and the mass transport coefficient was higher ($9.7\ 10^{-5}$ m s^{-1}) along with the diffusivity ($7.3\ 10^{-9}$ m^2 s^{-1}), which led to enhanced electrosorption rates. Afterward, an optimal electrode potential was obtained (-1.1 V vs. Ag/AgCl), while higher voltages led to faradaic reactions. Moreover, the adsorption capacity was lower (123 mg g^{-1}) than that of electrosorption (170 mg g^{-1}) and was even higher (307 mg g^{-1}) with actual effluents. This was probably due to the influence of electromigration, which was confirmed by new models that could predict the electrosorption kinetics well considering mass transport and acid dissociation constants.

Keywords: Phenolic compounds; Activated carbon beads; Capacitive current; Fixed-bed column reactor; Modeling

1. Introduction

The release of olive mill wastewater (OMWW) into the aquatic environment is a major issue (Azzam and Hazaimeh, 2021; Esteves et al., 2021; Haddad et al., 2021; Lissaneddine et al., 2021a). These effluents are toxic; they have a high inorganic salt content (electrical conductivity ~ 5–23 mS cm^{-1}) (Aharonov-Nadborny et al., 2016; Lissaneddine et al., 2021a) and a high organic load, i.e., high chemical oxygen demand (COD) (~ 110 g-O_2 L^{-1}) (Taylor et al., 2015). They are especially saturated with aromatic molecules, particularly phenolic compounds (PCs). They pose a serious environmental problem due to their phytotoxicity, which inhibits the activity of plants and microorganisms (Elayadi et al., 2021, 2019). PCs also affect surface water and groundwater, threatening aquatic life and altering soil quality (Elayadi et al., 2021). Moreover, hazardous OMWW is concentrated in a short period of time each year since it is a seasonal activity. However, PCs also represent added-value molecules at reliable doses that can be recovered for subsequent valorization in the pharmaceutical, cosmetic and food industries (Annab et al., 2019). Several physical, chemical, biological or combined technologies have been proposed to remove PCs, including separation methods (e.g., adsorption, membrane separation and ion exchange) and degradation techniques such as advanced oxidation processes (e.g., electro-Fenton, heterogeneous photocatalysis)(Brillas and Garcia-Segura, 2020; Genethliou et al., 2020; He et al., 2020; Lissaneddine et al., 2021a; Mousset, 2020; Mousset et al., 2021, 2018b, 2017, 2016a; Tundis et al., 2020; Ververi and Goula, 2019; Yue et al., 2019a). Separation technologies offer the possibility to recover these added-value compounds under specific applied conditions instead of degrading them. Electrosorption is gaining particular attention (Macías-garcía et al., 2019; Sahin et al., 2020) due to its advantages of selectivity, desorption control and low energy requirements (Sahin et al., 2020; Yang et al., 2021). Electrode materials are of primary importance in such an electrochemical system because they impact the electrosorption rates and yields. These

characteristics depend on the specific surface area, pore size distribution, electric conductivity, surface function and wettability (Lissaneddine et al., 2021b; Sun et al., 2016; Yue et al., 2019b). Three-dimensional (3D) particle electrodes provide a large electroactive surface area and can be easily implemented in fixed-bed reactors to favor mass transfer (Andrés García et al., 2018; Lissaneddine et al., 2021b; Macías-garcía et al., 2019; Yue et al., 2019b). Recently, 3D particle electrodes were shown to exhibit advantages in providing additional active sites and enhanced mass transfer compared to two-dimensional (2D) electrodes, which is conducive to improving the removal efficiency (Wang et al., 2021). Various 3D and bio-sourced materials have been employed for adsorption technologies. For instance, alginate offers advantages, as it acts as an embedding medium to assist in the preparation of easily separating and recycling adsorbents (Xu et al., 2021). It allows the implementation of powdered materials that have a larger specific surface area than granular adsorbents without the need for a postfiltration step to remove the fine adsorbent particles. Many researchers have employed beads with alginate coatings on several kinds of adsorbent materials, such as activated carbon (AC) (Girijan et al., 2021), or functionalized them to be more efficient (Wadhawan et al., 2020). These composite beads have been tested to remove organic pollutants in wastewater (Khan et al., 2021; Xu et al., 2021). In our recent article, bio-sourced beads based on a mixture of sodium alginate (SA) and powdered AC (SA-AC) made from olive pomace waste were used for the elimination of PCs from OMWW by adsorption (Lissaneddine et al., 2021a). However, pollutant transport within the beads is limited with such technology. This phenomenon should be less limited when electrosorption is used, as electromigration is favored, for example. To the best of the authors' knowledge, the interesting properties of alginate composite beads have not previously been tested for electrosorption.

Moreover, different studies have already demonstrated the performance of 3D electrodes for the electrosorption of organic compounds (e.g., acid red 88, orange II, methylene blue and metribuzin) from wastewater (Lissaneddine et al., 2021b). Matrix effects have rarely been considered, while a supporting electrolyte has always been added in electrosorption experiments (Lissaneddine et al., 2021b). However, matrix effects are known to interfere with the electrochemical process efficiency, and the addition of salts constitutes a supplementary source of pollution (Lissaneddine et al., 2021b; Mousset, 2020; Mousset et al., 2020, 2019, 2018a). Moreover, the few existing models of organic electrosorption do not include the physico-chemical properties of the compounds or mass transport phenomena, although they are of primary importance in the process efficiency (Lissaneddine et al., 2021b).

It is within this context that a detailed investigation has been carried out for the first time to understand and predict the electrosorption of PCs from simulated and actual OMWW. The prepared SA-AC beads were newly implemented as a 3D electrode for electrosorption experiments. The effect of the main parameters, i.e., the electrode preparation (crosslinking agent and AC content) and experimental conditions (applied electrode potential), on the electrosorption kinetics and capacity are stated in detail. In addition, novel theoretical models are proposed to predict the evolution of the electrosorption of organic compounds in simulated and real effluents, considering the mass transport and difference in acid dissociation constants (pKa) of the PCs.

2. Experimental

2.1. Effluent preparation and characterization

Two kinds of effluents were studied: one was a simulated OMWW that was used to optimize the operating parameters, and the second was an actual OMWW. The latter was employed to study the matrix effect by comparison with the simulated effluent.

Simulated OMWW was prepared using potassium chloride (KCl) (6 g L^{-1}) and phenol (4 g L^{-1}) and adjusted to pH 4 using hydrochloric acid (HCl) (Sigma Aldrich, Saint-Quentin-Fallavier, France) to be representative of the average characteristics of actual OMWW (Lissaneddine et al., 2021a). The phenol content was determined by UV–visible spectrophotometry (Shimadzu UV-2600 spectrophotometer) at the maximum absorption wavelength of 269 nm (Adebayo and Areo, 2021).

Real OMWW was collected from modern oil mills located in the region of Marrakech in Morocco during the olive oil extraction season from December to March in the 2020/2021 campaign when the main products were PCs (Lissaneddine et al., 2021a). The main characteristics were pH = 4.8, $[Cl^-]$ = 8.5 g L^{-1}, conductivity = 16 mS cm^{-1}, and total PCs = 10.6 mg L^{-1}; details of the characteristics are described elsewhere (Lissaneddine et al., 2021a). The total PC content was measured by the Folin-Ciocalteu method using meta-phosphoric acid, petroleum ether, ethyl acetate and methanol as reagents (Sigma Aldrich, Saint-Quentin-Fallavier, France) (Singleton, V. L., & Rossi, 1965). All commercially available reagents were used without further purification, while ultrapure water (18.2 MΩ cm) (PureLab ELGA Classic, Veolia Water, Antony, France) was used in all experiments and analyses.

2.2. Preparation and characterization of the 3D porous electrode

The porous material (SA-AC beads) was prepared based on activated carbon of olive pomace according to a previous paper (Lissaneddine et al., 2021a). First, a mixture of a hydrogel of

sodium alginate (BioChemica) (1%) was fabricated at 60 °C. Second, AC powder was added to the alginate hydrogel with constant stirring for 24 h to obtain a homogeneous dispersion. Next, the dispersed solution was poured dropwise into a crosslinking solution for bead solidification. The presence of a crosslinking agent leads to competition between the gelling reaction and polyelectrolyte complex, which also results in the formation of a more porous gel (Mi et al., 2002). Two crosslinking agents (iron(III) (Fe) and calcium(II) (Ca)) were used in bead preparation, both at 100% weight per volume (% w/v). The proportions in % w/v of AC (0%, 0.5%, 0.75%, 1%, 2%, and 3%) were varied in the SA-AC bead preparation process. The surface area (Brunauer-Emmett-Teller (BET) analysis), surface morphology (scanning electron microscopy (SEM)), elemental composition (energy-dispersive X-ray spectroscopy (EDS)) and surface function (Fourier transform infrared spectroscopy (FTIR)) of the initial beads have been described previously (Lissaneddine et al., 2021a).

The electrochemical properties of the prepared SA-AC beads electrode were evaluated using a potentiostat (AMETEK, Massy, France) in a three-electrode system whose design is described in Section 2.3. The SA-AC beads, a graphite rod and a Ag/AgCl electrode were employed as the working electrode, counter electrode and reference electrode, respectively. The electroactive surface of the porous material was determined by cyclic voltammetry (CV) with -0.2 to 0.8 V vs. Ag/AgCl as the voltage range and 0.01 V s^{-1} as the scan rate. The electroactive surface area (A in cm^2) was calculated according to the Randles-Sevcik equation (Eq. 1) from the peak currents determined with the polarization curve (Mousset et al., 2016b).

$$I_P = 2.69 \times 10^5 \times AD^{1/2} n^{3/2} \gamma^{1/2} C \quad (1)$$

where I_p is the peak current (in A), n is the number of electrons participating in the redox reaction (n=1), D is the diffusion coefficient of $[Fe(CN)_6]^{3-}$ (7.60×10^{-6} cm^2 s^{-1}), C is the concentration of $[Fe(CN)_6]^{3-}$ (1×10^{-5} mol cm^{-3}) and γ is the scan rate.

Tafel slopes were obtained from linear sweep voltammetry (LSV) with -2 to 2 V vs. Ag/AgCl as the voltage range and 0.01 V s^{-1} as the scan rate and were used to calculate the exchange current density (I_0) of the 3D porous electrode (Adnan et al., 2021b; Fang et al., 2017; Mousset et al., 2016b). Electrochemical impedance spectroscopy (EIS) using the frequency range from 50,000 to 0.1 Hz and an amplitude of 10 mV was performed to characterize the working electrode/electrolyte interface using the equivalent electrical circuit (EEC) method (Mousset et al., 2016b). The EIS data were fitted using ZSimpWin data analysis software (AMETEK, Massy, France).

2.3. Electrochemical setup and procedure

The electrosorption performance achieved with the SA-AC beads working electrode was tested on a fixed-bed column reactor (2.6 cm internal diameter) (Fig. 1) using a graphite rod (210 mm length, 12 mm diameter) (Final Advanced Material, Didenheim, France) as a current collector to connect SA-AC beads (35 g) with the potentiostat in monopolar mode. The average particle size of the SA-AC beads was 2 mm, and the height of the bed electrode was 9 cm. The counter electrode was a graphite rod (100 length, 8 mm diameter) (Final Advanced Material, Didenheim, France) and was considered the anode. A nonconductive polytetrafluoroethylene (PTFE) mesh (with a pore diameter of 1 mm) was placed between the cathode and the anode to avoid contact in between without interfering with the electrosorption mechanism. In all experiments, 100 mL of effluent was introduced with ascending flow using a peristaltic pump (Fisher Scientific, Illkirch-Graffenstaden, France) at a constant flow rate of 10 mL min^{-1}. The cathode potential was varied from -0.8 to -1.3 V vs. Ag/AgCl, and the open circuit (OC) was tested for the blank experiment in the absence of an applied voltage. The electrosorption capacity (q in mg g^{-1}) was calculated according to Eq. 2 (Li et al., 2016):

$$q = \frac{(C_0 - C_e)\,V}{m} \quad (2)$$

where C_0 and C_e are the initial and equilibrium concentrations of the pollutant, respectively (mg L^{-1}), V is the volume of the circulated solution (L), and m is the adsorbent mass of the SA-AC electrode (g).

The mass transfer coefficients (k_m) within the column were determined by LSV using the limiting-current technique with solutions containing 0.05 M $K_3Fe(CN)_6$, 0.10 M $K_4Fe(CN)_6$ and 0.50 M Na_2CO_3 (Sigma Aldrich, Saint-Quentin-Fallavier, France) (Adnan et al., 2021b; Cañizares et al., 2006; Selman and Tobias, 1978). The internal ohmic resistances were determined according to Eq. 3 (Adnan et al., 2022; Miller et al., 2019):

$$\sum RI = E_{cell} - |E_C| - |E_A| \quad (3)$$

where ∑RI is the ohmic drop, E_{cell} is the cell voltage, and $|E_A|$ and $|E_C|$ are the absolute values of the anode and cathode potentials, respectively.

The electroactivity of phenol (4 g L^{-1}) was assessed by LSV performed from -2 to 2 V vs. Ag/AgCl at 0.01 V s^{-1} scan rate using KCl (6 g L^{-1}) as the supporting electrolyte. This was performed to determine whether the direct electroreduction and/or electrooxidation of phenol could occur.

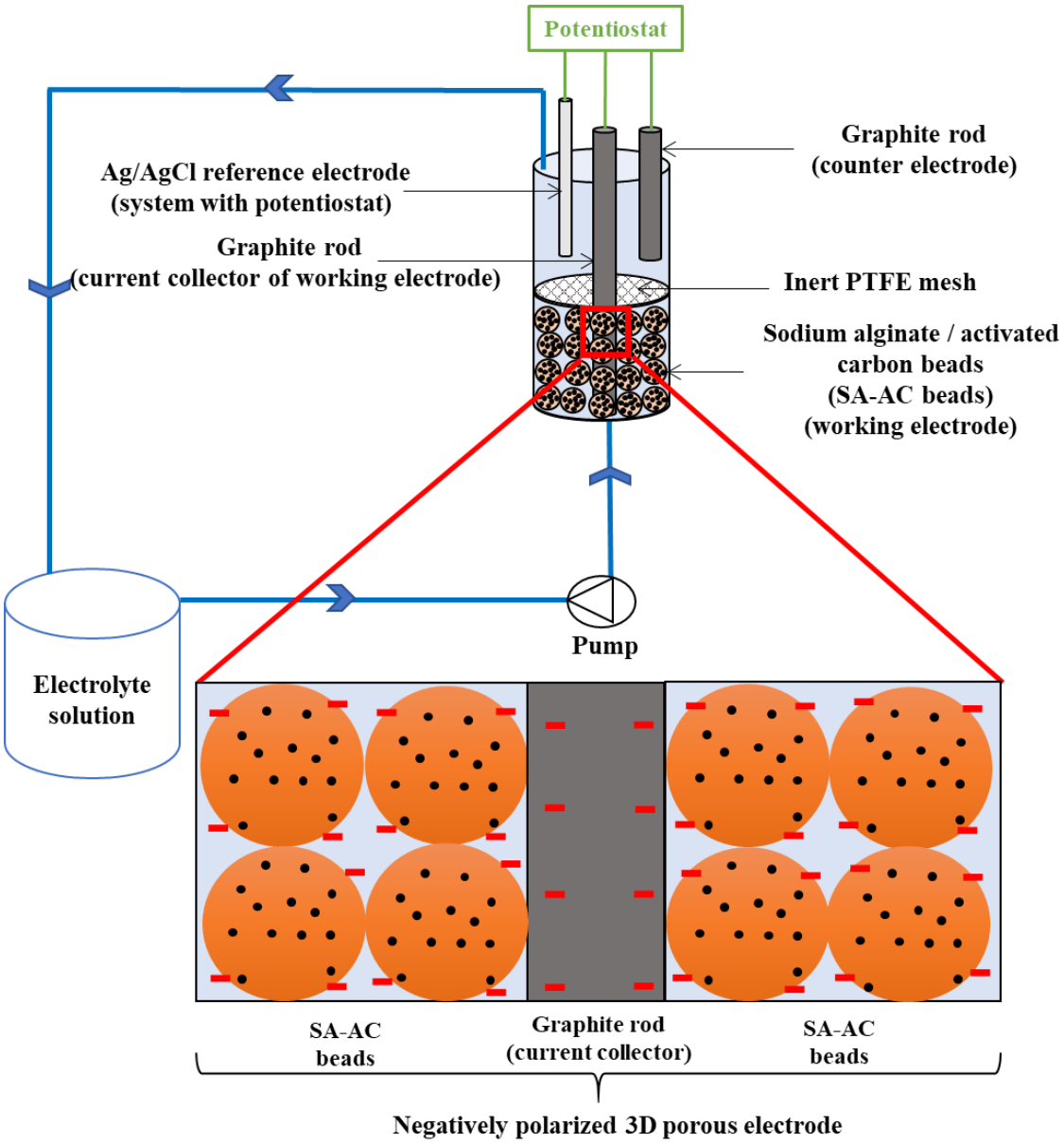

Fig. 1. Fixed-bed electrosorption schematic setup.

2.4. Modeling

A new model was proposed to predict the rate of phenol electrosorption onto beads by incorporating the transport phenomena defined by the Nernst–Planck equation (Jasielec, 2021) that include diffusion, electromigration and convection. Electromigration was neglected with the simulated effluent since the phenol molecule (pKa = 9.95) is uncharged at the applied pH of 4. Although the setup is under forced convection within the column, the low flow rate

would imply that the diffusion of phenol toward the 3D porous material does not occur in the stationary regime. Supposing that the beads are all spherical and have the same diameter (~ 3.5 mm), the phenol rate toward the 3D porous material (r_c) can obey Fick's law under the transient regime according to Eq. 4 (Miomandre et al., 2005):

$$r_c = -\frac{1}{S}\frac{dC}{dt} = \frac{1}{V}(C_t - C_t^{el})\sqrt{\frac{D}{\pi t}} \quad (4)$$

where D is the diffusion coefficient of phenol, S is the specific surface area of the beads, t is time, and C_t and C_t^{el} are the concentrations of phenol in the solution and at the electrode surface at time t, respectively.

C_t^{el} can be expressed as a function of C_0, as follows:

$$C_t^{el} = C_0 - C_{t-1} \quad (5)$$

where C_{t-1} and C_0 are the concentrations of phenol at time t-1 and t = 0 (in min), respectively, in the discrete model.

Then, $C_t - C_t^{el}$ can be expressed according to Eq. 6:

$$C_t - C^{el} = C_t + C_{t-1} - C_0 \quad (6)$$

After incorporating Eq. 5 into Eq. 4 and integrating Eq. 4 from $C_t = C_0$ to C_t, Eq. 7 can be obtained:

$$\ln(C_t + C_{t-1} - C_0) = \frac{2S\sqrt{D}}{\pi V} t^{\frac{1}{2}} + \ln(C_0) \quad (7)$$

When dealing with real effluents (OMWW), a mixture of PCs with different pKa values (3.0–4.0 to 10.0–11.0) should be considered (Lissaneddine et al., 2021a). Therefore, the influence of the electromigration of ionic PCs must be added to Eq. 4:

$$r_c = -\frac{1}{S}\frac{dC}{dt} = \frac{1}{V}(C_t - C_t^{el})\sqrt{\frac{D}{\pi t}} + j_k \quad (8)$$

with

$$j_k = \frac{F}{RT} Z_k D_k C_k E = \frac{F}{RT} Z_k D_k C_k \rho_s j_{app} \quad (9)$$

where $j_k, D_{k,} Z_k$ and C_k are the flux, diffusion coefficient, valence and concentration of the charged PCs (k), respectively; R is the gas constant; T is the absolute temperature; F is the Faraday constant; E is the electric field; ρ_s is the solution resistivity; and j_{app} is the applied current density.

After integrating Eq. 8 from $C_t = C_0$ to C_t, Eq. 10 can be obtained:

$$t^{\frac{1}{2}} = \frac{X+\sqrt{X^2-4YZ}}{2Y} \quad (10)$$

with

$$X = \frac{2S\sqrt{D}}{\pi V} \quad (11)$$

$$Y = \frac{FZ_k D_k \rho_s j_{app}}{RT} \quad (12)$$

$$Z = ln\left(\frac{C_t + C_{t-1} - C_0}{C_0(C_t - C_0)}\right) \quad (13)$$

The fittings of the models with experimental results were evaluated with the root mean square error (RMSE) as written in Eq. 14 (Adnan et al., 2021a):

$$RMSE = \sqrt{\frac{\sum_{i=1}^{K}(y_i - y_i')^2}{K}} \quad (14)$$

where y_i' is the experimental value, y_i is the model value and K is the number of iterated values.

The lower the RMSE value is, the more suitable the model.

3. Results and discussion

3.1. Electrochemical characterization of the 3D porous electrodes

The electrochemical properties of the initial SA-AC beads electrodes were determined to evaluate their electrochemical performance as an active electrode material. The electroactive surface area (I_0), charge transfer resistance (R_{CT}) and electrical double-layer capacitance (C_{DL}) values were not impacted by the content of AC in the beads. Therefore, only their average values were reported.

The electroactive surface area of porous electrodes determines the number of polarized active sites, which in turn determines the rate and yield of electrosorption. In addition, the electroactive surface area is a key parameter for the electrosorption efficiency (Zhu and Zhao, 2019). CV showed that the beads possessed a large electroactive surface area of $23 \times 10^3 \pm 5.5 \times 10^3$ cm^2 (Fig. 2a). Comparatively, previous studies estimated surfaces with areas of 0.14 cm^2 with an oxidized activated carbon electrode (Deryło-Marczewska et al., 2019), 0.93 cm^2 with an AC nanotube-supported palladium electrode (Wang et al., 2010) and 531 cm^2 with an activated carbon fiber electrode (Ergan and Gengec, 2020). The value obtained with SA-AC emphasized that the encapsulation of AC in the beads allowed a large electroactive surface area to be maintained compared to porous electrodes proposed in the literature. This is of prime interest to achieve high electrosorption capacity. This is in agreement with the adsorption ability of SA-AC beads determined in a previous study, in which the BET specific surface area of SA-AC beads was 523 m^2 g^{-1} and the porous nature of the adsorbent was shown (total pore volume of 0.308 cm^3 g^{-1}), as confirmed by FTIR, SEM and EDS

(Lissaneddine et al., 2021a). I_0 was determined to evaluate the catalytic performance of the electrode and electron transfer across the electrode (Sharma et al., 2013; Situmorang et al., 2020). The I_0 calculated from the Tafel slopes was 3.24 mA (Fig. 2b). This value was high compared to the values of electrodes based on other materials described in the literature, such as activated carbon derived from rice husk (0.06 to 0.17 mA) (Jiao et al., 2020) and ammonium bicarbonate and activated carbon (0.084 to 1.5 mA) (Li et al., 2014). Knowing that a higher I_0 leads to a quicker response to a change in potential (Sharma et al., 2013; Sun and Chen, 2016), better electrode performance is expected.

To further characterize the porous electrode/electrolyte interface, EIS data were obtained after validation of impedance spectra with the linear Kramers-Kronig transform (KKT) technique (Fasmin and Srinivasan, 2015) (Fig. 2c). The chi-squared residues (χ^2) calculated by using the KKT technique to fit the experimental spectra and the Randle-type EEC model for fitting along with KKT were determined to be $1.5\ 10^{-5}$ and $9.3\ 10^{-7}$, respectively. Among all the EEC models tested, the best agreement with EIS spectra was obtained with the Randle-type circuit model shown in Fig. 3. This model further demonstrated that exchanges with the electrolyte occur directly within the SA-AC beads, not at the bead and current collector surfaces. This can also explain why the parameters related to the electrode/electrolyte interface (electroactive surface area, I_0, R_{CT} and C_{DL}) were relatively constant, regardless of the AC load within the beads. The associated R_{CT} and C_{DL} values of the EEC model were 1.7± 0.7 Ω and 0.15 ± 0.084 µF cm^{-2}, respectively. R_{CT} was low compared with R_{CT} values of other reported porous electrodes, such as almond shell-based activated nanoporous carbon (5.8 Ω) (Jain and Tripathi, 2014), activated carbon (4.2 Ω) (Tian et al., 2020) and Cu_2O-doped activated carbon (9.39 Ω) (Zhang et al., 2015). This trend of R_{CT} compared with other porous materials corroborated the higher I_0 value in the present case. This would therefore promote electrosorption on the SA-AC beads electrodes. In addition, a higher C_{DL} value was found

289 compared to that of activated carbon (0.0058 μF cm^{-2}) (Tian et al., 2020), which should
290 increase the electric double layer and, therefore, the electrosorption efficiency (Lissaneddine
291 et al., 2021b). This is discussed in the next subsection.

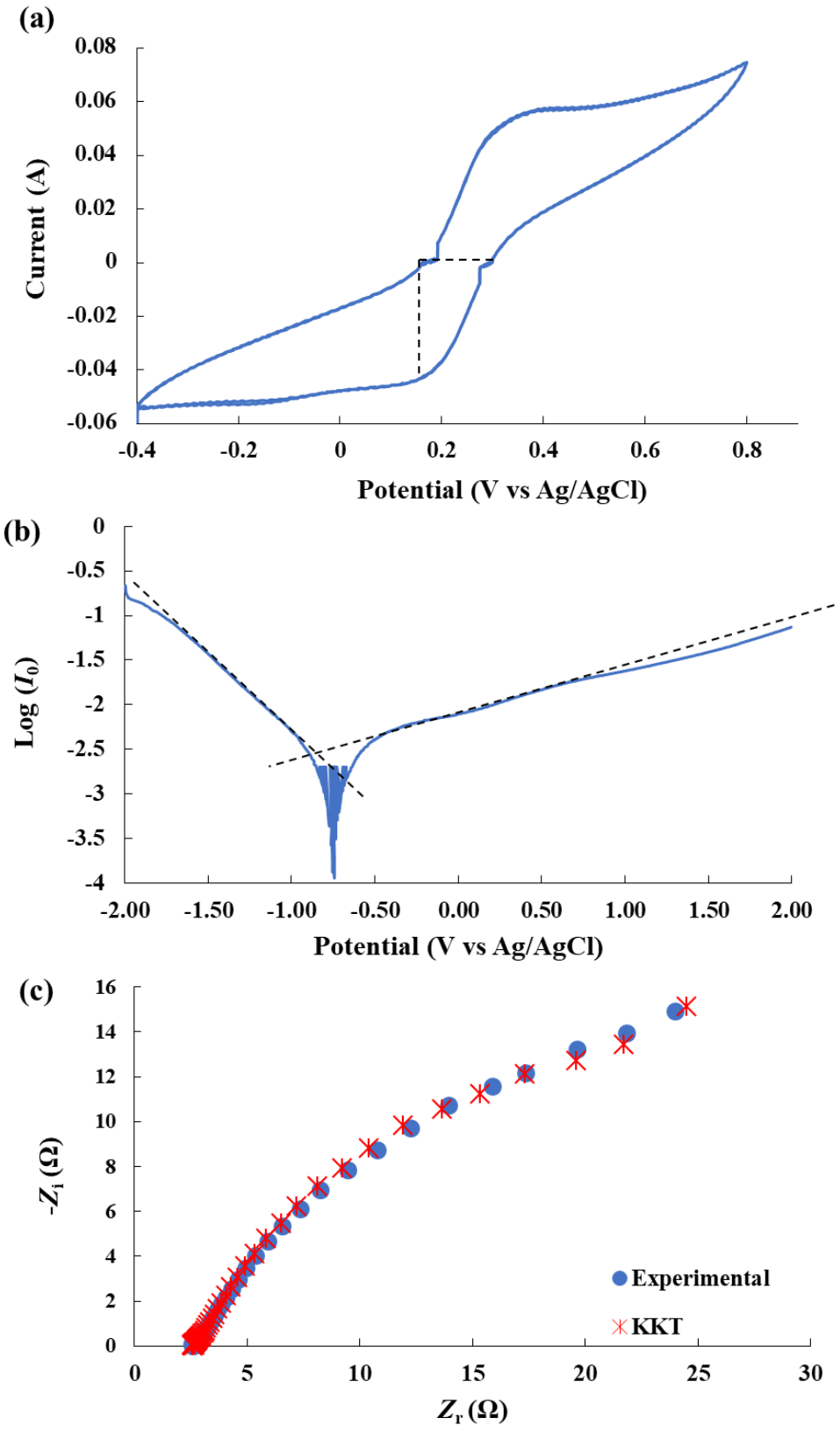

292

293 **Fig. 2.** Electrochemical properties of the prepared SA-AC beads electrode using CV (a), LSV

294 (b) and EIS (c).

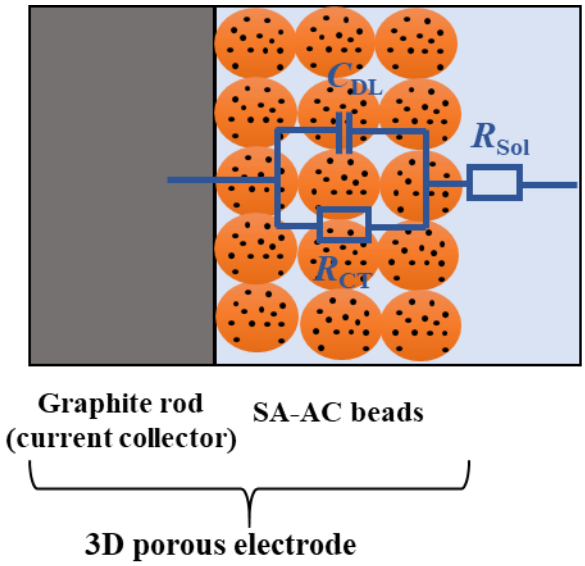

295

296 **Fig. 3.** Scheme of the EEC model integrated into the 3D porous electrodes.

297

298 ### 3.2. Electrosorption efficiency

299 #### 3.2.1. Effect of the iron and calcium contents in the beads

300 To optimize the stability of the bio-sourced adsorbent during electrosorption, iron or calcium
301 was added to the beads during preparation (Fig. 4). The results show that the electrosorption
302 capacities were similar, on the order of 204 ± 3 mg g^{-1} and 197 ± 10 mg g^{-1} after 240 min for
303 Fe and Ca, respectively.

304 To select the optimal element, the electrical conductivities of the two porous electrodes (Fe
305 and Ca) were compared by EIS measurements. Fig. 4b illustrates the Nyquist representations.
306 The R_{CT} values were ranked as follows: Fe (1.7 Ω) < Ca (2.6 Ω). The R_{CT} value of Fe is 1.5-
307 fold less than that of Ca, highlighting a slight increase in electrode conductivity achieved with
308 Fe. This trend was assumed to be due to differences in electron hopping, polarons and ionic
309 radii. The transition energy between Fe^{2+} and Fe^{3+} is 0.2 eV (Iqbal and Farooq, 2007), which
310 indicates pronounced electron hopping and, hence, a rapid increase in conductivity with iron.
311 Similar results have been observed in a previous study involving doping magnesium

aluminate with divalent and trivalent metal ions. The magnesium aluminate doped by Fe^{3+} had lower resistivity, i.e., higher conductivity, than that doped with Ca^{2+} (Iqbal and Farooq, 2007). This is because the ionic radius of Ca^{2+} (0.99 Å) is larger than that of Fe^{3+} (0.64 Å) and the small polaron and electron hopping achieved with iron (Iqbal and Farooq, 2007).

This can further explain why in this study, beads prepared with Fe displayed slightly higher electrosorption capacities. Since the increase in material conductivity has previously been demonstrated to increase the electrosorption efficiency (Lissaneddine et al., 2021b), the selected optimal element of crosslinking agent used for beads preparation was Fe.

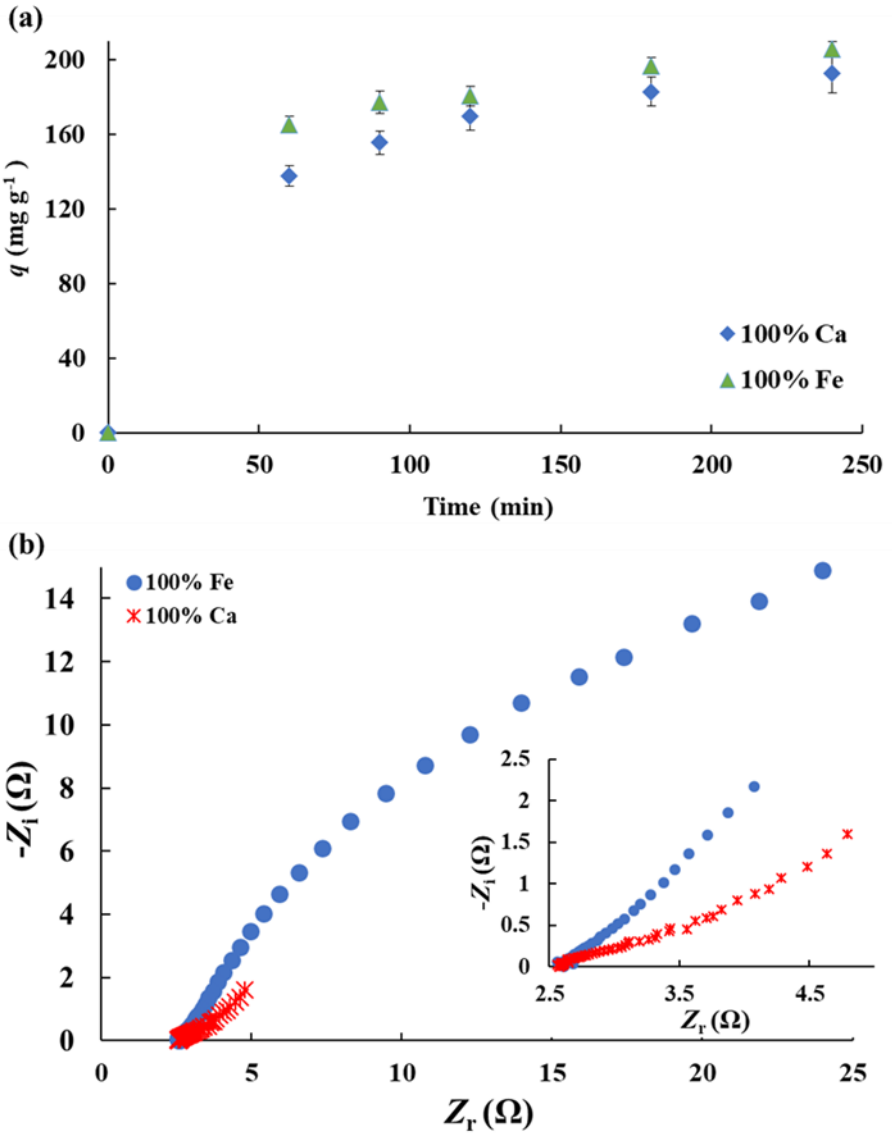

321

322 **Fig. 4.** Effect of the presence of iron or calcium in beads preparation on the electrosorption
323 efficiency of phenol (a) and on the electrode conductivity estimated from the Nyquist plot (b).
324 The operating conditions were as follows: anode: graphite rod; cathode: graphite rod and 35 g
325 SA-1% w/v AC beads; cathode potential: -1.2 V vs. Ag/AgCl; electrolyte: 6 g L^{-1} KCl and 4 g
326 L^{-1} phenol; flow rate: 10 mL min^{-1}; and m/V = 0.35 g mL^{-1}.

327

328 ### 3.2.2. Influence of AC percentage

329 The influence of AC percentage, i.e., the adsorbent dose, on phenol electrosorption kinetics in
330 simulated OMWW is illustrated in Fig. 5a. First, the electrosorption capacity increased

rapidly over time as the active sites became accessible. With increasing time, the active sites tended to be saturated so that the electrosorption capacity slowly increased until adsorption equilibrium was finally reached. Second, the electrosorption capacity increased for all percentages of AC tested with increasing time. In addition, there was an increase in electrosorption capacity with increasing percentages of AC up to 1% w/v (183 mg g^{-1}). This trend was in agreement with the literature, in which the phenol adsorption capacity increased with increasing powdered AC content in alginate gels (Jodra and Mijangos, 2003). Moreover, a further increase in the percentage of AC (3% w/v) led to a decline in the electrosorption capacity of phenol to 178 mg g^{-1}.

Interestingly, the trend of k_m evolution with AC percentages (Fig. 5b) was similar to the behavior of phenol electrosorption (Fig. 5a). The k_m values increased from 8.9 10^{-5} m s^{-1} for 0% w/v AC to 9.7 10^{-5} m s^{-1} for 1% w/v AC and decreased to 8.1 10^{-5} m s^{-1} for 3% w/v AC. This further confirmed that electrosorption occurred mainly within the beads, as suggested by the EEC model (Section 3.1), not at the graphite rod and bead interfaces. Moreover, this suggests that the electrosorption capacity strongly depended on the diffusivity of the phenol within the beads. It has been previously shown that when AC particles are trapped in SA gels, the PCs diffuse into the micropores of the SA gels and are adsorbed by the AC enveloped in the SA matrix (Chung et al., 2003). The increase in the amount of AC could then increase the diffusivity and, therefore, the mass transport. At an AC content that is too high (3% w/v), AC may agglomerate, which could lead to a reduction in the elasticity of the hydrogel network and the formation of a denser network (Thakur, 2018; Tiwari et al., 2012). In a previous adsorption work, AC agglomerated in the beads, which led to an increase in the diffusional path length and a decrease in the adsorption capacity (Araga et al., 2017; Iqbal et al., 2016). In addition, the mass transfer coefficient has been shown to decrease with increasing adsorbent particle size (Krishna, M. S., Raju, G. J., & Rao, 1966). These statements agree with the

decreased electrosorption capacity of phenol at 3% w/v AC. To better visualize the mechanism of electrosorption with an increase in AC content within the beads, a scheme is proposed in Fig. 6. This drawing highlights the constant external diffusion layer regardless of AC content, while the internal diffusion within the beads is affected. Mass transport is then influenced along with the electrosorption efficiency.

Furthermore, increasing the percentage of AC possibly decreased the internal ohmic resistance of the SA-AC bead electrode from 2.9 V (0% w/v AC) to 2.2 V (1% w/v AC) (Fig. 5c), which subsequently resulted in a higher electrosorption capacity. A further increase in AC content (3% w/v AC) led to an increase in $\sum RI$ to 2.7 V. The reasons for this latter trend could be explained as follows. The mass transport coefficient decreased for 3% w/v AC (Fig. 5b), and according to the results of Fang et al. (2005, 2006), the delayed transport of the ions into electrode (modified activated carbon aerogel) pores resulted in an increase in the internal ohmic resistance (Fang et al., 2005; Fang and Binder, 2006). Consequently, the AC percentage influenced ion transport and the internal ohmic resistance. Bian et al. (2016) demonstrated that the electrosorption performance significantly improved with a decrease in the electrode's internal ohmic resistance (14 to 3.6 Ω) for inorganic compounds on a membrane capacitive deionization reactor (Bian et al., 2016). This was further evidenced in this study for organic compound electrosorption on a fixed-bed column reactor with beads electrode. To conclude, $\sum RI$ seemed to be correlated with mass transport as well as the AC content in the beads and the related electrosorption efficiency.

Based on these results, the optimum percentage of AC was taken as 1% w/v for the next electrosorption experiments.

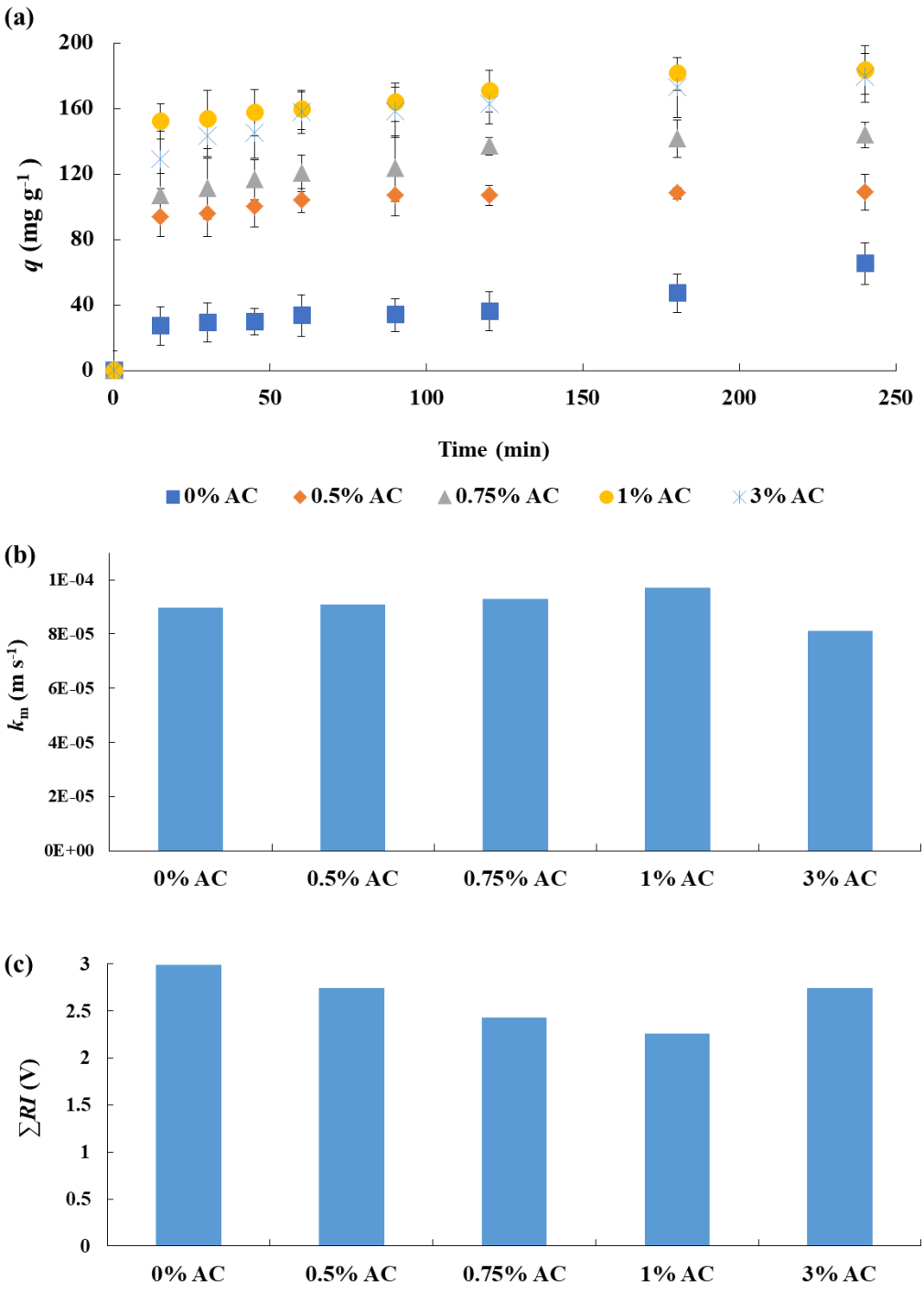

379

380 **Fig. 5.** Effect of AC percentage (% w/v) on the evolution of the electrosorption capacity of
381 phenol (a), mass transport (b) and internal ohmic resistance (c). The operating conditions were
382 as follows: anode: graphite rod; cathode: graphite rod and 35 g SA (100% Fe)-AC beads;
383 cathode potential: -1.2 V vs Ag/AgCl; electrolyte: 6 g L^{-1} KCl and 4 g L^{-1} phenol; flow rate:
384 10 mL min^{-1}; and m/V = 0.35 g mL^{-1}.

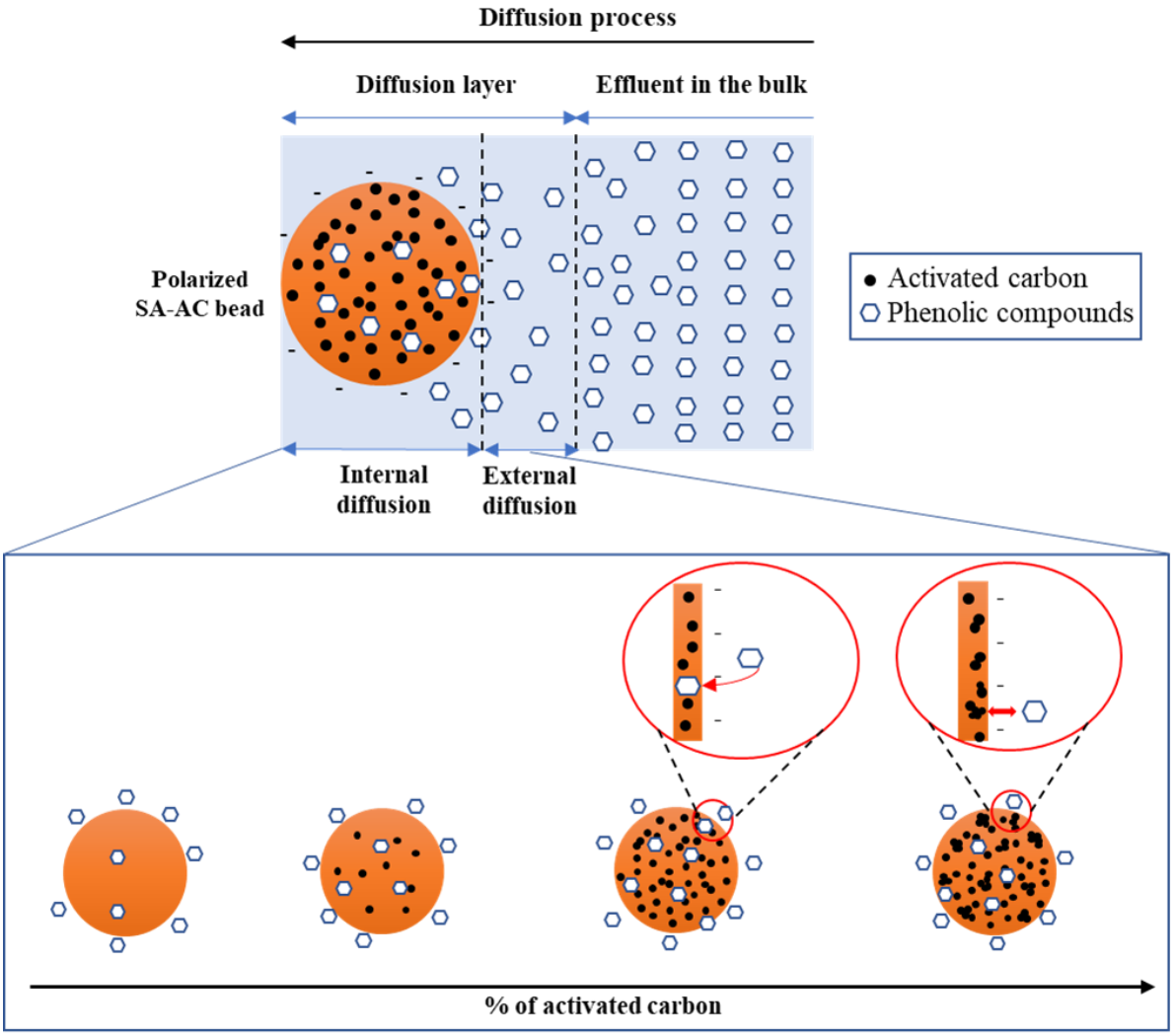

Fig. 6. Mechanism of phenol electrosorption in SA-AC beads with increasing AC content.

3.2.3. Effect of the cathode potential

The electrode potential is the driving force of the electrosorption efficiency. Preliminary experiments were performed by applying an anode potential and using the beads as the working electrode. However, the beads could not support the high voltage involved under oxidation conditions, meaning that they were not stable (data not shown). Subsequent experiments were therefore performed by applying a cathode potential. The influence of varying the cathode potential from -0.8 to -1.3 V vs. Ag/AgCl on the phenol electrosorption efficiency compared to the OC condition is shown in Fig. 7. The electrosorption capacity

increased with decreasing applied potential from -0.8 to -1.2 V vs. Ag/AgCl, reaching a maximum electrosorption capacity of 170 mg g^{-1} at equilibrium (Fig. 7a). It has been previously demonstrated that the potential can impact the electrosorption capacity of uncharged molecules (Gileadi, 1966), which was the case for phenol (pKa = 9.95) considering a solution pH of 4. However, the electrosorption capacity decreased to 73 mg g^{-1} when the applied potential equaled -1.3 V vs. Ag/AgCl. At this range of cathode potentials, water (H_2O) reduction starts to occur according to Eq. (15), in which hydrogen gas (H_2) is produced on the surface of the 3D electrode (Ziati and Hazourli, 2019).

$$2H_2O + 2e^- \rightarrow H_2 + 2OH^- \quad (15)$$

This H_2 electrogeneration reaction limits the availability of the active sites on the cathode surface (Adnan et al., 2021a; Hazourli et al., 1996). The involvement of this faradaic reaction therefore strongly reduced the electrosorption capacity to 73 mg g^{-1}, which was even lower than that under OC conditions (123 mg g^{-1}). In this latter case, the absence of electric current emphasized the gain (38%) obtained with electrosorption at optimal voltage compared with the adsorption mechanism alone. To further assess whether electrooxidation or electroreduction of phenol can occur, an LSV curve was plotted in the presence of phenol and KCl (Fig. 7b). Neither reduction nor oxidation peaks could be observed between -2 and 2 V vs. Ag/AgCl. This means that no electron transfer occurred between phenol and the electrodes. Thus, it was assumed that only capacitive phenomena were involved (i.e., electrosorption including adsorption). Uncharged molecules such as phenol at pH 4 can electrosorb because electrode polarization induces the replacement of solvent molecules with the organic compound at the interface (Gileadi, 1966). This enhances electrosorption (Gileadi, 1966).

419 The energy requirement is an important economic parameter to consider in electrosorption
420 process optimization. Considering the electrosorption efficiency as a function of specific
421 charge values (Fig. 7c), decreasing the applied potential increased the specific charge. The
422 maximum electrosorption capacity (approximately 170 mg g^{-1}) was only reached after 0.28
423 Ah L^{-1} at -1.1 V vs. Ag/AgCl, compared to 2 Ah L^{-1} at -1.2 V vs. Ag/AgCl. This means that
424 the energy requirement would be 7 times lower at -1.1 V vs Ag/AgCl.

425 Thus, the applied cathode potential was -1.1 V vs. Ag/AgCl for the next electrosorption
426 experiment with real OMWW.

427

428

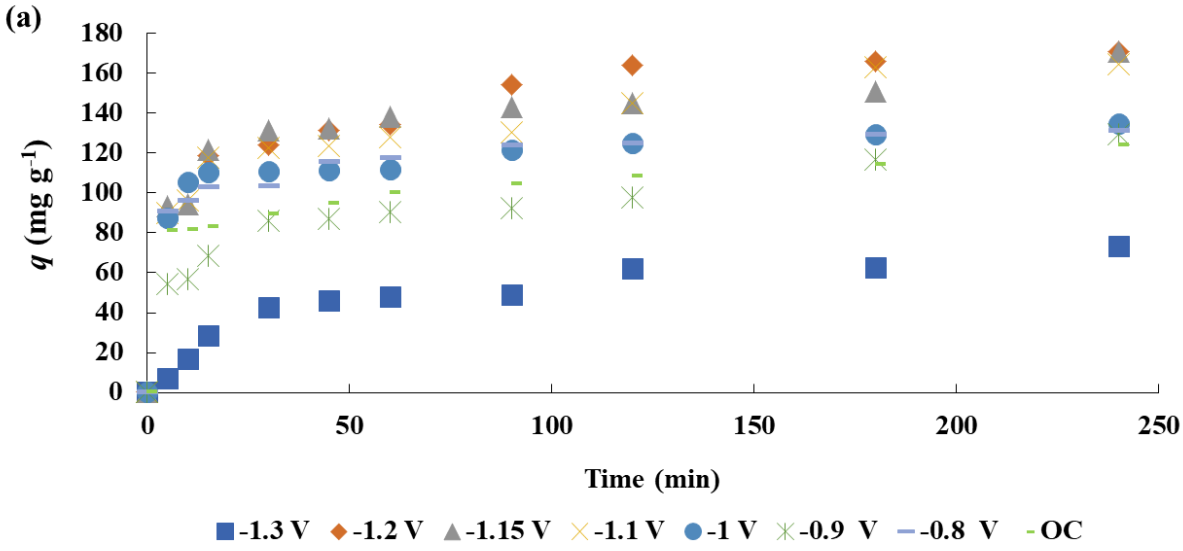
(a)
q (mg g-1)
Time (min)
-1.3 V
-1.2 V
-1.15 V
-1.1 V
-1 V
-0.9 V
-0.8 V
OC

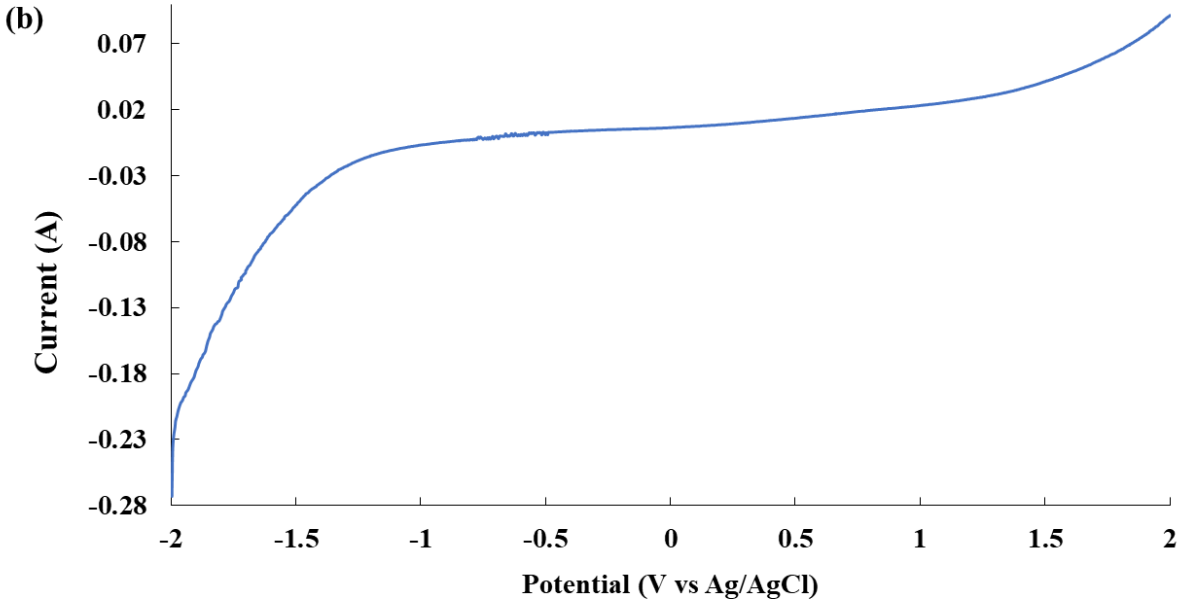
(b)
Current (A)
Potential (V vs Ag/AgCl)

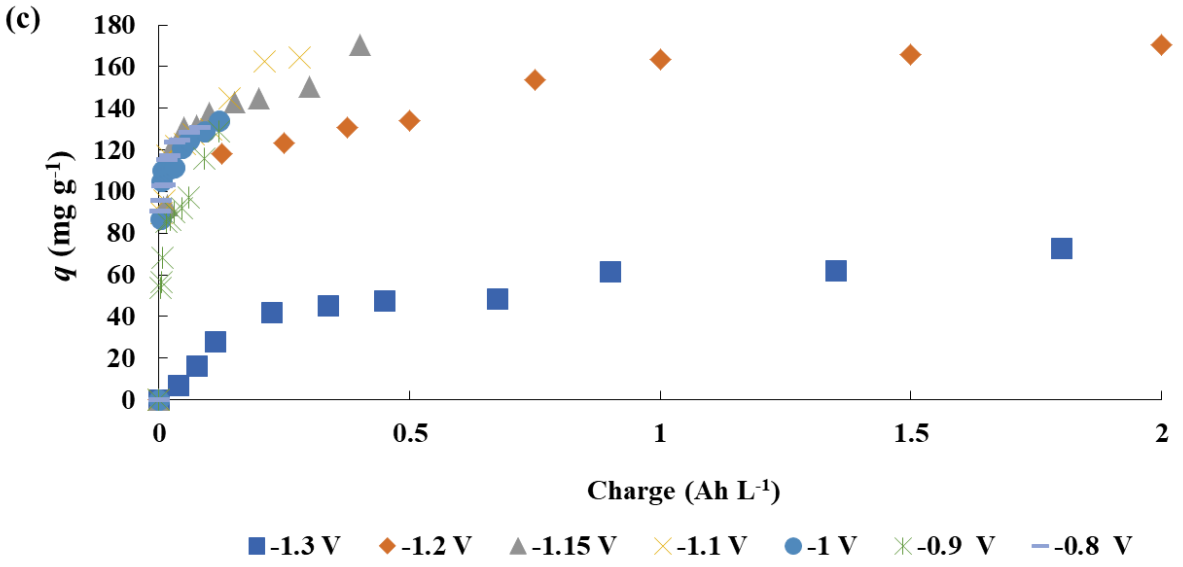
(c)
q (mg g-1)
Charge (Ah L-1)
-1.3 V
-1.2 V
-1.15 V
-1.1 V
-1 V
-0.9 V
-0.8 V

429

Fig. 7. Effect of cathode potential (V vs. Ag/AgCl) on phenol electrosorption considering the contact time (a), LSV with SA-AC beads as the working electrode (b), and effect of cathode potential on specific charge (c). Operating conditions: anode: graphite rod; cathode: graphite rod and 35 g SA (100% Fe)-1% w/v AC beads; electrolyte: 6 g L^{-1} KCl and 4 g L^{-1} phenol; flow rate: 10 mL min^{-1}; and m/V = 0.35 g mL^{-1}.

3.2.4. Multicomponent effect with actual effluent

Electrosorption experiments with real OMWW were carried out under optimal conditions: 1% w/v AC, 100% w/v Fe and -1.1 V vs. Ag/AgCl cathode potential (Fig. 8). The results showed that the maximum electrosorption capacity of PCs was higher (307 mg g^{-1}) than that with phenol solutions (164 mg g^{-1}) in simulated OMWW. This difference could be explained by the presence of multiple PCs with different physico-chemical properties, such as diverse pKa values. The main PCs identified in actual OMWW have been listed in a previous paper (Lissaneddine et al., 2021a), and their pKa values ranged from 3.0-4.0 to 10.0-11.0. Since the pH of the solution was between 4 and 5, the compounds, whose pKa values are equal to or below this pH value, predominantly exist in their acidic form. In contrast, the PCs, whose pKa is higher than the solution pH, primarily exist in their basic form. In addition, it is usually assumed that the acidic forms of the PCs remain uncharged because the hydroxyl (OH/O^-) and carboxyl ($COOH/COO^-$) groups are protonated. In contrast, their basic forms are ionized since these groups are deprotonated (Baransi et al., 2012; Liu et al., 2020). The charged PCs were therefore subjected to electromigration in addition to diffusion near the electrode. Although the SA-AC beads surfaces was negatively charged (cathode), electrostatic repulsion between the negatively charged PCs and the negatively charged SA-AC beads surfaces could still promote contact with the beads (Parida and Pradhan, 2010). The electrostatic repulsion could also be explained by the molecular complexation of PCs in OMWW. The polarizability of

PCs depends on the combination of dispersion interactions and hydrophobic effects, which is the main driving force for the molecular complexation of PCs in OMWW (Bouknana et al., 2019). In addition, since the hydraulic flow of the negative fixed-bed electrode is less than that of the positive counter electrode, electromigration can also favor the contact of PCs within the fixed-bed electrode before reaching the anode. Therefore, the electrosorption rates and yields were maximized. The influence of electromigration was previously observed with other organic compounds (e.g., acid red 88, orange II, and methylene blue) in simulated effluents (Lissaneddine et al., 2021b; Sun et al., 2016; Yue et al., 2019b). The present results newly demonstrated the influence of electromigration with a multicomponent system containing organics in an actual effluent.

Based on this trend, the SA-AC beads electrode can be used to separate not only phenol but also other PCs (47%) from actual OMWW by electrosorption for subsequent valorization in future research studies.

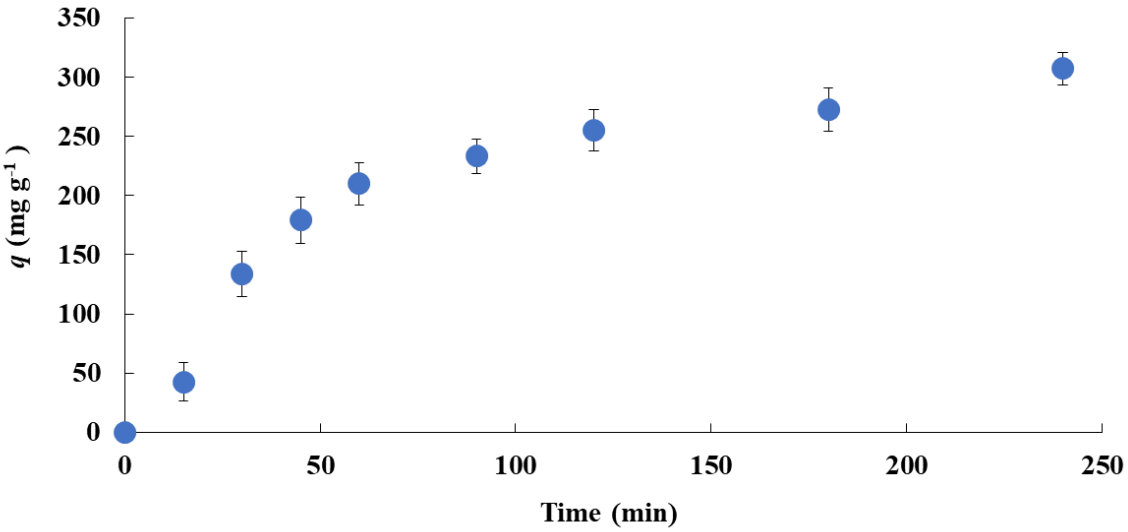

Fig. 8. Effect of contact time on the electrosorption of PCs from real OMWW under optimal operating conditions. Operating conditions: anode: graphite rod; cathode: graphite rod and 35

g SA (100% Fe)-1% w/v AC beads; cathode potential: -1.1 V vs. Ag/AgCl; flow rate: 10 mL min^{-1}; and m/V ratio = 0.35 g mL^{-1}.

3.3. Theoretical evolution of organic compound electrosorption in simulated and actual effluents

The models developed in Section 2.4 were used to predict the electrosorption evolution of phenol in simulated OMWW as a function of AC content (Fig. 9a) and PCs in real OMWW (Fig. 9b). All the RMSE values were lower than 2.95×10^{-2}, which confirmed the good agreement of the model with the experimental data. Thus, diffusion in simulated effluent and diffusion along with electromigration in real effluent are the main phenomena involved in the kinetics of organic compound electrosorption.

The good fitting with real effluent data further supported the estimated average valence of ionic PCs, which was 3.8. This value was obtained by weighting the valence of each PC charged in solution at a pH of 4.8 based on the ratio of their basic form to their average concentration in real effluent. The main ionic PCs identified in actual OMWW were gallic acid (valence of 5), ferulic acid (valence of 5), caffeic acid (valence of 4), cinnamic acid (valence of 2), and coumaric acid (valence of 3) according to a previous study (Lissaneddine et al., 2021a).

Furthermore, based on the slope values ($\frac{2S\sqrt{D}}{\pi V}$) of $\ln(C_t + C_{t-1} - C_0)$ = f($t^{1/2}$) (Eq. 7), the diffusivity constant for phenol could be estimated as a function of AC content ($D_{X\%}$) as follows (Eq. 16):

$$D_{X\%} = \frac{\pi V^2}{4S^2} \quad (16)$$

The evolution of $D_{X\%}$ as a function of AC content is plotted in Fig. 9c. The trend followed that of the electrosorption capacity of phenol at different AC percentages (Fig. 5a), i.e.,

optimal diffusion (7.3 10^{-9} m^2 s^{-1}) at 1% w/v AC. This was also consistent with the k_m value evolution (Fig. 5b). This further corroborated the fact that the electrosorption capacity strongly depended on the diffusivities of the PCs within the beads.

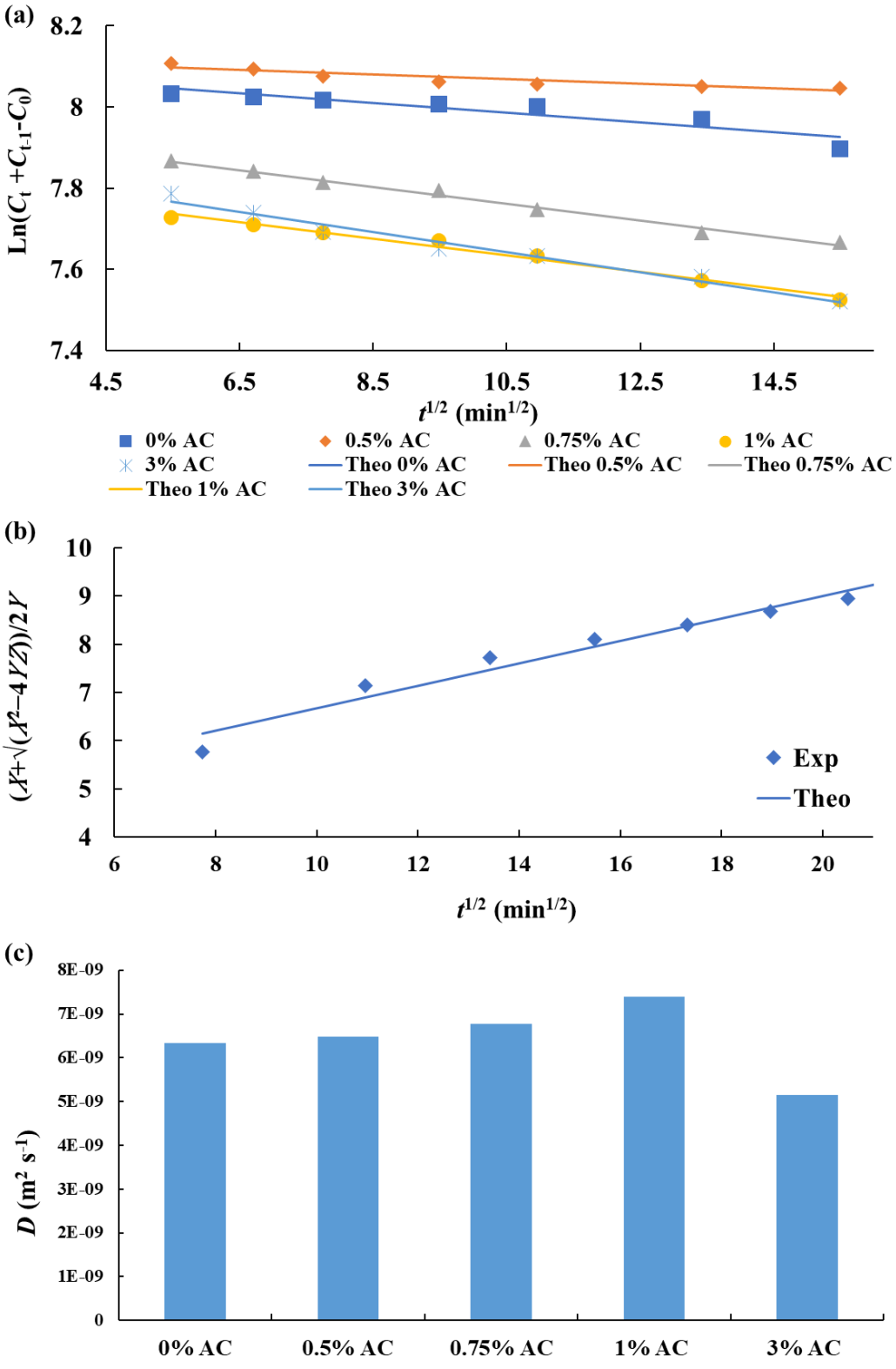

Fig. 9. Experimental (symbol) versus theoretical correlations (continuous line) as a function of $t^{1/2}$ in simulated OMWW as a function of AC content (a) and PCs in real OMWW and (b) effect of the percentage of AC on the diffusion coefficient (c).

Conclusions

This study proposed a novel approach to remove PCs from simulated and actual OMWW by implementing electrosorption onto SA-AC beads as porous bio-sourced electrodes. The impacts of key parameters (crosslinking agent (iron and calcium), AC content and cathode potential) on the removal efficiency of PCs were explored. The main new insights are listed as follows:

- The higher conductivity obtained with the Fe crosslinking agent led to a slightly higher electrosorption efficiency than that obtained with Ca.
- The AC content within the beads impacted the mass transfer and diffusion coefficients as well as the internal ohmic resistance. An optimal AC amount was observed (1% w/v) because an excessively high concentration implied agglomeration.
- A cathode potential of -1.1 V vs. Ag/AgCl was found to be optimal considering the electrosorption capacity and energy requirements. Too high voltage leads to faradaic reactions that hamper the electrosorption mechanism. Electrosorption was better than adsorption efficiency, while uncharged phenol electrosorption could still occur.
- The electrosorption efficiency was higher with real wastewater than with simulated effluent. This could be due to the presence of multiple organic components that have different pKa values.
- New discrete models were proposed to understand and predict the electrosorption efficiency. The kinetics were mainly limited by diffusion in the transient regime in the

synthetic effluent, while the electromigration of ionic PCs also impacted electrosorption with real OMWW.

- The results of the EEC model along with the kinetic models confirmed that electrosorption mainly occurred within the beads, not at the 3D electrode/electrolyte interface, unlike what is often assessed.

The good electrosorption efficiency obtained for PCs removal from OMWW is promising for PCs recovery for subsequent valorization. The reusability of porous electrodes is also an important indicator when evaluating the electrosorption performance of materials. Since the organic compounds were trapped in the beads, electrosorption may be more irreversible and, therefore, desorption may be less easy. This is the subject of incoming research that will provide a more detailed evaluation of the particle cathode stability and reusability. A further possibility is to combine electrosorption for recovery with a degradation process for the elimination of unwanted compounds, which is also the subject of ongoing research.

Acknowledgments

This work was funded by the PHC TOUBKAL 2019 Project (French-Morocco bilateral program, grant number 41525VG). The authors would like to thank the National Center for Studies and Research on Water and Energy (Cadi Ayyad University_Morocco) and Laboratoire Réactions et Génie des Procédés (LRGP), CNRS/Université de Lorraine (France), and the European regional development fund program (CPER SusChemProc) for their technical and scientific support of this work.

References

Adebayo, M.A., Areo, F.I., 2021. Removal of phenol and 4-nitrophenol from wastewater using a composite prepared from clay and Cocos nucifera shell: Kinetic, equilibrium and thermodynamic studies. Resour. Environ. Sustain. 3, 100020. https://doi.org/10.1016/j.resenv.2021.100020

Adnan, F.H., Mousset, E., Pontvianne, S., Pons, M., 2021a. Mineral cathodic electro-precipitation and its kinetic modelling in thin-film microfluidic reactor during advanced electro-oxidation process. Electrochim. Acta 387, 138487. https://doi.org/10.1016/j.electacta.2021.138487

Adnan, F.H., Pons, M.-N., Mousset, E., 2021b. Mass transport evolution in microfluidic thin film electrochemical reactors: New correlations from millimetric to submillimetric interelectrode distances. Electrochem. commun. 130, 107097. https://doi.org/10.1016/j.elecom.2021.107097

Adnan, F.H., Pontvianne, S., Pons, M.N., Mousset, E., 2022. Unprecedented roles of submillimetric interelectrode distances and electrogenerated gas bubbles on mineral cathodic electro-precipitation: Modeling and interface studies. Chem. Eng. J. 431. https://doi.org/10.1016/j.cej.2021.133413

Aharonov-Nadborny, R., Raviv, M., Graber, E.R., 2016. Soil spreading of liquid olive mill processing wastes impacts leaching of adsorbed terbuthylazine. Chemosphere 156, 220–227. https://doi.org/10.1016/j.chemosphere.2016.04.104

Andrés García, E., Agulló-Barceló, M., Bond, P., Keller, J., Gernjak, W., Radjenovic, J., 2018. Hybrid electrochemical-granular activated carbon system for the treatment of greywater. Chem. Eng. J. 352, 405–411. https://doi.org/10.1016/j.cej.2018.07.042

566 Annab, H., Fiol, N., Villaescusa, I., Essamri, A., 2019. Journal of Environmental Chemical
567 Engineering A proposal for the sustainable treatment and valorisation of olive mill
568 wastes. J. Environ. Chem. Eng. 7, 102803. https://doi.org/10.1016/j.jece.2018.11.047

569 Araga, R., Soni, S., Sharma, C.S., 2017. Fluoride adsorption from aqueous solution using
570 activated carbon obtained from KOH-treated jamun (Syzygium cumini) seed. J. Environ.
571 Chem. Eng. 5, 5608–5616. https://doi.org/10.1016/j.jece.2017.10.023

572 Azzam, M.O.J., Hazaimeh, S.A., 2021. Olive mill wastewater treatment and valorization by
573 extraction/concentration of hydroxytyrosol and other natural phenols. Process Saf.
574 Environ. Prot. 148, 495–523. https://doi.org/10.1016/j.psep.2020.10.030

575 Baransi, K., Dubowski, Y., Sabbah, I., 2012. Synergetic effect between photocatalytic
576 degradation and adsorption processes on the removal of phenolic compounds from olive
577 mill wastewater. Water Res. 46, 789–798. https://doi.org/10.1016/j.watres.2011.11.049

578 Bian, Y., Liang, P., Yang, X., Jiang, Y., Zhang, C., Huang, X., 2016. Using activated carbon
579 fiber separators to enhance the desalination rate of membrane capacitive deionization.
580 Desalination 381, 95–99. https://doi.org/10.1016/j.desal.2015.11.016

581 Bouknana, D., Jodeh, S., Sbaa, M., Hammouti, B., 2019. A phytotoxic impact of phenolic
582 compounds in olive oil mill wastewater on fenugreek "Trigonella foenum-graecum."
583 Environ. Monit. Assess.

584 Brillas, E., Garcia-Segura, S., 2020. Benchmarking recent advances and innovative
585 technology approaches of Fenton, photo-Fenton, electro-Fenton, and related processes: A
586 review on the relevance of phenol as model molecule. Sep. Purif. Technol. 237, 116337.
587 https://doi.org/10.1016/j.seppur.2019.116337

588 Cañizares, P., Marcos, I.F. De, Rodrigo, M.A., Lobato, J., 2006. Measurement of mass-

589 transfer coefficients by an electrochemical technique. J. Chem. Educ. 83, 1204–1207.
590 https://doi.org/10.1021/ed083p1204

591 Chung, T., Tseng, H., Juang, R., 2003. Mass transfer effect and intermediate detection for
592 phenol degradation in immobilized Pseudomonas putida systems 38, 1497–1507.
593 https://doi.org/10.1016/S0032-9592(03)00038-4

594 Deryło-Marczewska, A., Skrzypczyńska, K., Kuśmierek, K., Świątkowski, A., Zienkiewicz-
595 Strzałka, M., 2019. The adsorptive properties of oxidized activated carbons and their
596 applications as carbon paste electrode modifiers. Adsorption 25, 357–366.
597 https://doi.org/10.1007/s10450-019-00016-6

598 Elayadi, F., Adlouni, C. El, Achak, M., Herradi, E. El, Krati, M. El, Tahiri, S., 2019. Effects
599 of raw and treated olive mill wastewater (OMW) by coagulation- flocculation , on the
600 germination and the growth of three plant species (wheat , white beans , lettuce).
601 Moroccan J. Chem. 1, 111–122.

602 Elayadi, F., Boumya, W., Achak, M., Chhiti, Y., 2021. Experimental and modeling studies of
603 the removal of phenolic compounds from olive mill wastewater by adsorption on
604 sugarcane bagasse. Environ. Challenges 4, 100184.
605 https://doi.org/10.1016/j.envc.2021.100184

606 Ergan, B.T., Gengec, E., 2020. Dye degradation and kinetics of online Electro-Fenton system
607 with thermally activated carbon fiber cathodes. J. Environ. Chem. Eng. 8, 104217.
608 https://doi.org/10.1016/j.jece.2020.104217

609 Esteves, B.M., Morales-Torres, S., Maldonado-Hódar, F.J., Madeira, L.M., 2021. Integration
610 of olive stones in the production of Fe/AC-catalysts for the CWPO treatment of synthetic
611 and real olive mill wastewater. Chem. Eng. J. 411.
612 https://doi.org/10.1016/j.cej.2021.128451

Fang, B., Binder, L., 2006. A modified activated carbon aerogel for high-energy storage in electric double layer capacitors. J. Power Sources 163, 616–622. https://doi.org/10.1016/j.jpowsour.2006.09.014

Fang, B., Wei, Y.Z., Maruyama, K., Kumagai, M., 2005. High capacity supercapacitors based on modified activated carbon aerogel. J. Appl. Electrochem. 35, 229–233. https://doi.org/10.1007/s10800-004-3462-6

Fang, Z., Cao, X., Li, Xuexiao, Wang, H., Li, Xianning, 2017. Bioresource Technology Electrode and azo dye decolorization performance in microbial-fuel-cell- coupled constructed wetlands with different electrode size during long- term wastewater treatment. Bioresour. Technol. 238, 450–460. https://doi.org/10.1016/j.biortech.2017.04.075

Fasmin, F., Srinivasan, R., 2015. Detection of nonlinearities in electrochemical impedance spectra by Kramers–Kronig Transforms. J. Solid State Electrochem. 19, 1833–1847. https://doi.org/10.1007/s10008-015-2824-9

Genethliou, C., Kornaros, M., Dailianis, S., 2020. Biodegradation of olive mill wastewater phenolic compounds in a thermophilic anaerobic upflow packed bed reactor and assessment of their toxicity in digester effluents. J. Environ. Manage. 255, 109882. https://doi.org/10.1016/j.jenvman.2019.109882

Gileadi, E., 1966. Electrosorption of uncharged molecules on solid electrodes. J. Electroanal. Chem. 11, 137–151. https://doi.org/10.1016/0022-0728(66)80073-6

Girijan, S., Kumar, M., Gomber, S., 2021. Starch and powdered activated carbon amended alginate-biomass beads for metronidazole and bulk organic matter removal: Synthesis, optimization, reaction kinetics and reusability. J. Environ. Chem. Eng. 9, 106102. https://doi.org/10.1016/j.jece.2021.106102

637 Haddad, K., Jeguirim, M., Jellali, S., Thevenin, N., Ruidavets, L., Limousy, L., 2021. Biochar
638 production from Cypress sawdust and olive mill wastewater: Agronomic approach. Sci.
639 Total Environ. 752, 141713. https://doi.org/10.1016/j.scitotenv.2020.141713

640 Hazourli, S., Bonnecaze, G., Astruc, M., 1996. Adsorption et electrosorption de composes
641 organiques sur charbon actif en grains partie I - Influence du potentiel imposé et du
642 nombre de cycles adsorption and electrosorption of organic compounds on granular
643 activated carbon part I- Influence of applied. Environ. Technol. 17, 1275–1283.
644 https://doi.org/10.1080/09593330.1996.9618457

645 He, F., Hemmatifar, A., Bazant, M.Z., Hatton, T.A., 2020. Selective adsorption of organic
646 anions in a flow cell with asymmetric redox active electrodes 1–26.

647 Iqbal, M., Iqbal, N., Bhatti, I.A., Ahmad, N., Zahid, M., 2016. Response surface methodology
648 application in optimization of cadmium adsorption by shoe waste: A good option of
649 waste mitigation by waste. Ecol. Eng. 88, 265–275.
650 https://doi.org/10.1016/j.ecoleng.2015.12.041

651 Iqbal, M.J., Farooq, S., 2007. Effect of doping of divalent and trivalent metal ions on the
652 structural and electrical properties of magnesium aluminate. Mater. Sci. Eng. B Solid-
653 State Mater. Adv. Technol. 136, 140–147. https://doi.org/10.1016/j.mseb.2006.09.009

654 Jain, A., Tripathi, S.K., 2014. Almond shell-based activated nanoporous carbon electrode for
655 EDLCs. https://doi.org/10.1007/s11581-014-1282-1

656 Jasielec, J.J., 2021. Electrodiffusion Phenomena in Neuroscience and the Nernst–Planck–
657 Poisson Equations. Electrochem 2, 197–215.
658 https://doi.org/10.3390/electrochem2020014

659 Jiao, Y., Hu, Y., Han, L., Zhou, M., 2020. Activated Carbon Derived from Rice Husk as

660 Efficient Oxygen Reduction Catalyst in Microbial Fuel Cell. Electroanalysis 32, 2969–
661 2975. https://doi.org/10.1002/elan.202060409

662 Jodra, Y., Mijangos, F., 2003. Phenol adsorption in immobilized activated carbon with
663 alginate gels phenol adsorption in immobilized activated. Sep. Sci. Technol. 37–41.
664 https://doi.org/10.1081/SS-120019412

665 Khan, A.S., Ibrahim, T.H., Khamis, M.I., Nancarrow, P., Iqbal, J., AlNashef, I., Jabbar, N.A.,
666 Hassan, M.F., Mjalli, F.S., 2021. Preparation of sustainable activated carbon-alginate
667 beads impregnated with ionic liquid for phenol decontamination. J. Clean. Prod. 128899.
668 https://doi.org/10.1016/j.jclepro.2021.128899

669 Krishna, M. S., Raju, G. J., & Rao, C. V., 1966. Mass Transfer in Packed Beds in Annuli
670 Electrolytic Redox Reactions. Period. Polytech. Chem. Eng. 11, 95–102.

671 Li, D., Qu, Y., Liu, J., He, W., Wang, H., Feng, Y., 2014. Using ammonium bicarbonate as
672 pore former in activated carbon catalyst layer to enhance performance of air cathode
673 microbial fuel cell. J. Power Sources 272, 909–914.
674 https://doi.org/10.1016/j.jpowsour.2014.09.053

675 Li, Y., Zhang, C., Jiang, Y., Wang, T., Wang, H., 2016. Effects of the hydration ratio on the
676 electrosorption selectivity of ions during capacitive deionization. Desalination 399, 171–
677 177. https://doi.org/10.1016/j.desal.2016.09.011

678 Lissaneddine, A., Mandi, L., Achaby, M. El, Mousset, E., Eldon, R., Ouazzani, N., Pons, M.,
679 Aziz, F., 2021a. Performance and dynamic modeling of a continuously operated pomace
680 olive packed bed for olive mill wastewater treatment and phenol recovery. Chemosphere
681 130797. https://doi.org/10.1016/j.chemosphere.2021.130797

682 Lissaneddine, A., Pons, M.-N., Aziz, F., Ouazzani, N., Mandi, L., Mousset, E., 2021b. A

683 critical review on the electrosorption of organic compounds in aqueous effluent –
684 Influencing factors and engineering considerations. Environ. Res. J. Under revision.

685 Liu, B., Zhong, F., Yokoyama, W., Huang, D., Zhu, S., Li, Y., 2020. Interactions in starch co-
686 gelatinized with phenolic compound systems: effect of complexity of phenolic
687 compounds and amylose content of starch. Carbohydr. Polym. 116667.
688 https://doi.org/10.1016/j.carbpol.2020.116667

689 Macías-garcía, A., Carrasco-amador, J.P., Encinas-sánchez, V., Díaz-díez, M.A., 2019.
690 Preparation of activated carbon from kenaf by activation with H 3 PO 4 . Kinetic study
691 of the adsorption / electroadsorption using a system of supports designed in 3D , for
692 environmental applications. J. Environ. Chem. Eng. 7, 103196.
693 https://doi.org/10.1016/j.jece.2019.103196

694 Mi, F., Sung, H., Shyu, S., 2002. Drug release from chitosan ± alginate complex beads
695 reinforced by a naturally occurring cross-linking agent. Carbohydr. Polym. 48, 61–72.

696 Miller, A., Singh, L., Wang, L., Liu, H., 2019. Linking internal resistance with design and
697 operation decisions in microbial electrolysis cells. Environ. Int. 126, 611–618.
698 https://doi.org/10.1016/j.envint.2019.02.056

699 Miomandre, F., Sadki, S., Audebert, P., Méallet-Renault, R., 2005. Electrochimie - Des
700 concepts aux applications. Dunod, Paris. (in French), Paris.

701 Mousset, E., 2020. Unprecedented reactive electro-mixing reactor: Towards synergy between
702 micro- and macro-reactors? Electrochem. commun. 118, 106787.
703 https://doi.org/10.1016/j.elecom.2020.106787

704 Mousset, E., Frunzo, L., Esposito, G., van Hullebusch, E.D., Oturan, N., Oturan, M.A., 2016a.
705 A complete phenol oxidation pathway obtained during electro-Fenton treatment and

validated by a kinetic model study. Appl. Catal. B Environ. 180, 189–198. https://doi.org/10.1016/j.apcatb.2015.06.014

Mousset, E., Loh, W.H., Lim, W.S., Jarry, L., Wang, Z., Lefebvre, O., 2021. Cost comparison of advanced oxidation processes for wastewater treatment using accumulated oxygen-equivalent criteria. Water Res. 200, 117234. https://doi.org/https://doi.org/10.1016/j.electacta.2021.138466

Mousset, E., Pontvianne, S., Pons, M.-N., 2018a. Fate of inorganic nitrogen species under homogeneous Fenton combined with electro-oxidation/reduction treatments in synthetic solutions and reclaimed municipal wastewater. Chemosphere 201, 6–12. https://doi.org/10.1016/j.chemosphere.2018.02.142

Mousset, E., Puce, M., Pons, M.N., 2019. Advanced electro-oxidation with boron-doped diamond for acetaminophen removal from real wastewater in a microfluidic reactor: Kinetics and mass-transfer studies. ChemElectroChem 6, 2908–2916. https://doi.org/10.1002/celc.201900182

Mousset, E., Quackenbush, L., Schondek, C., Gerardin-Vergne, A., Pontvianne, S., Kmiotek, S., Pons, M.N., 2020. Effect of homogeneous Fenton combined with electron transfer on the fate of inorganic chlorinated species in synthetic and reclaimed municipal wastewater. Electrochim. Acta 334, 135608. https://doi.org/10.1016/j.electacta.2019.135608

Mousset, E., Wang, Z., Hammaker, J., Lefebvre, O., 2017. Electrocatalytic phenol degradation by a novel nanostructured carbon fiber brush cathode coated with graphene ink. Electrochim. Acta 258, 607–617. https://doi.org/10.1016/j.electacta.2017.11.104

Mousset, E., Wang, Z., Hammaker, J., Lefebvre, O., 2016b. Physico-chemical properties of pristine graphene and its performance as electrode material for electro-Fenton treatment

of wastewater. Electrochim. Acta 214, 217–230. https://doi.org/10.1016/j.electacta.2016.08.002

Mousset, E., Wang, Z., Olvera-Vargas, H., Lefebvre, O., 2018b. Advanced electrocatalytic pre-treatment to improve the biodegradability of real wastewater from the electronics industry — A detailed investigation study. J. Hazard. Mater. 360, 552–559. https://doi.org/10.1016/j.jhazmat.2018.08.023

Parida, K.M., Pradhan, A.C., 2010. Removal of phenolic compounds from aqueous solutions by adsorption onto manganese nodule leached residue. J. Hazard. Mater. 173, 758–764. https://doi.org/10.1016/j.jhazmat.2009.09.003

Sahin, E.M., Tongur, T., Ayranci, E., 2020. Removal of azo dyes from aqueous solutions by adsorption and electrosorption as monitored with in-situ UV-visible spectroscopy. Sep. Sci. Technol. 55, 3287–3298. https://doi.org/10.1080/01496395.2019.1676786

Selman, J.R., Tobias, C.W., 1978. Mass-transfer measurements by the limiting-current technique. Adv. Chem. Eng. 10, 211–318.

Sharma, M., Jain, P., Varanasi, J.L., Lal, B., Rodríguez, J., Lema, J.M., Sarma, P.M., 2013. Enhanced performance of sulfate reducing bacteria based biocathode using stainless steel mesh on activated carbon fabric electrode. Bioresour. Technol. 150, 172–180. https://doi.org/10.1016/j.biortech.2013.09.069

Singleton, V. L., & Rossi, J.A., 1965. Colorimetry of total phenolic substances. US Am. Chem. Soc. Symp. Ser. 26, 47–70.

Situmorang, R.S., Seri, O., Kawai, H., 2020. Estimation of exchange current density for hydrogen evolution reaction of copper electrode by using the differentiating polarization method. Appl. Surf. Sci. 505, 144300. https://doi.org/10.1016/j.apsusc.2019.144300

753 Sun, D., Chen, Y., 2016. Electrode kinetics of CO_2 electroreduction.
754 https://doi.org/10.1201/b20177-4

755 Sun, X.-F., Guo, B.-B., He, L., Xia, P.-F., Shu-Guang Wang, 2016. Electrically accelerated
756 removal of organic pollutants by a three-dimensional graphene aerogel. AIChE J. 59,
757 215–228. https://doi.org/10.1002/aic

758 Taylor, P., Ji, M., Jiang, X., Wang, F., 2015. Desalination and water treatment a mechanistic
759 approach and response surface optimization of the removal of oil and grease from
760 restaurant wastewater by electrocoagulation and electroflotation. Desalin. water Treat.
761 37–41. https://doi.org/10.1080/19443994.2014.929034

762 Thakur, S., 2018. Synthesis, characterization and adsorption studies of an acrylic acid-grafted
763 sodium nanocomposite. https://doi.org/10.1177/0263617417700636

764 Tian, X., Bao, S., Zhang, Y., 2020. Adsorption properties of V(IV) on the resin-activated
765 carbon composite electrodes in capacitive deionization. Int. J. Miner. Metall. Mater.

766 Tiwari, A., Soni, A., Bajpai, A.K., 2012. Nanoparticles loaded alginate beads as potential
767 adsorbent for removal of phenol from aqueous solution. Synth. React. Inorganic, Met.
768 Nano-Metal Chem. 42, 1158–1166. https://doi.org/10.1080/15533174.2012.682835

769 Tundis, R., Conidi, C., Loizzo, M.R., Sicari, V., Cassano, A., 2020. Olive Mill Wastewater
770 Polyphenol-Enriched Fractions by Integrated Membrane Process : A Promising Source
771 of Antioxidant , Hypolipidemic and Hypoglycaemic Compounds 1–15.

772 Ververi, M., Goula, A.M., 2019. Pomegranate peel and orange juice by-product as new
773 biosorbents of phenolic compounds from olive mill wastewaters. Chem. Eng. Process.
774 Process Intensif. 138, 86–96. https://doi.org/10.1016/j.cep.2019.03.010

775 Wadhawan, S., Jain, A., Nayyar, J., Kumar, S., 2020. Role of nanomaterials as adsorbents in

heavy metal ion removal from waste water: a review. J. water Process Eng. 33, 101038. https://doi.org/10.1016/j.jwpe.2019.101038

Wang, Y., Cui, C., Zhang, G., Xin, Y., Wang, S., 2021. Electrocatalytic hydrodechlorination of pentachlorophenol on Pd-supported magnetic biochar particle electrodes. Sep. Purif. Technol. 258, 118017. https://doi.org/10.1016/j.seppur.2020.118017

Wang, Y., Sheng, Z.M., Yang, H., Jiang, S.P., Li, C.M., 2010. Electrocatalysis of carbon black- or activated carbon nanotubes-supported Pd-Ag towards methanol oxidation in alkaline media. Int. J. Hydrogen Energy 35, 10087–10093. https://doi.org/10.1016/j.ijhydene.2010.07.172

Xu, S., Jin, Y., Li, R., Shan, M., Zhang, Y., 2021. Amidoxime modified polymers of intrinsic microporosity/alginate composite hydrogel beads for efficient adsorption of cationic dyes from aqueous solution. J. Colloid Interface Sci. https://doi.org/10.1016/j.jcis.2021.08.157

Yang, W., Zhou, M., Ma, L., 2021. A continuous flow-through system with integration of electrosorption and peroxi-coagulation for efficient removal of organics. Chemosphere 274, 129983. https://doi.org/10.1016/j.chemosphere.2021.129983

Yue, F., Zhang, Q., Xu, L., Zheng, Y., Yao, C., Jia, J., Leng, W., Hou, S., 2019a. Porous reduced graphene oxide/single-walled carbon nanotube film as freestanding and flexible electrode materials for electrosorption of organic dye. ACS Appl. nano Mater. 2, 6258–6267. https://doi.org/10.1021/acsanm.9b01236

Yue, F., Zhang, Q., Xu, L., Zheng, Y., Yao, C., Jia, J., Leng, W., Hou, S., 2019b. Porous reduced graphene oxide/single-walled carbon nanotube film as freestanding and flexible electrode materials for electrosorption of organic dye. ACS Appl. Nano Mater. 2, 6258–6267. https://doi.org/10.1021/acsanm.9b01236

Zhang, X., Li, K., Yan, P., Liu, Z., Pu, L., 2015. N-type Cu_2O doped activated carbon as catalyst for improving power generation of air cathode microbial fuel cells. Bioresour. Technol. 187, 299–304. https://doi.org/10.1016/j.biortech.2015.03.131

Zhu, P., Zhao, Y., 2019. Cyclic voltammetry measurements of electroactive surface area of porous nickel: Peak current and peak charge methods and diffusion layer effect. Mater. Chem. Phys. 233, 60–67. https://doi.org/10.1016/j.matchemphys.2019.05.034

Ziati, M., Hazourli, S., 2019. Experimental investigation of activated carbon prepared from date stones adsorbent electrode for electrosorption of lead from aqueous solution. Microchem. J. 146, 164–169. https://doi.org/10.1016/j.microc.2018.12.041

812

813